MITSUBISHI ELECTRIC RESEARCH LABORATORIES
https://www.merl.com

Quantum Diffusion Models for Few-Shot Learning

Wang, Ruhan; Wang, Ye; Liu, Jing; Koike-Akino, Toshiaki

TR2025-025 March 05, 2025

Abstract

Modern quantum machine learning (QML) methods involve the variational optimization of parameterized quantum circuits on training datasets, followed by predictions on testing datasets. Most state-of-the-art QML algorithms currently lack practical advantages due to their limited learning capabilities, especially in few-shot learning tasks. In this work, we propose three new frameworks employing quantum diffusion model (QDM) as a solution for the few-shot learning: label- guided generation inference (LGGI); label-guided denoising inference (LGDI); and label-guided noise addition inference (LGNAI). Experimental results demonstrate that our proposed algorithms significantly outperform existing methods.

AAAI Conference on Artificial Intelligence 2025

Mitsubishi Electric Research Laboratories, Inc.
201 Broadway, Cambridge, Massachusetts 02139

Quantum Diffusion Models for Few-Shot Learning

Ruhan Wang[1*], **Ye Wang**[2], **Jing Liu**[2], **Toshiaki Koike-Akino**[2]

[1]Indiana University Bloomington, 107 S Indiana Ave, Bloomington, IN 47405, USA
[2]Mitsubishi Electric Research Laboratories (MERL), 201 Broadway, Cambridge, MA 02139, USA
Email: {yewang, jiliu, koike}@merl.com

Abstract

Modern quantum machine learning (QML) methods involve the variational optimization of parameterized quantum circuits on training datasets, followed by predictions on testing datasets. Most state-of-the-art QML algorithms currently lack practical advantages due to their limited learning capabilities, especially in few-shot learning tasks. In this work, we propose three new frameworks employing quantum diffusion model (QDM) as a solution for the few-shot learning: label-guided generation inference (LGGI); label-guided denoising inference (LGDI); and label-guided noise addition inference (LGNAI). Experimental results demonstrate that our proposed algorithms significantly outperform existing methods.

Introduction

Quantum machine learning (QML) has emerged as a transformative tool for automated decision-making, influencing diverse fields such as finance, healthcare, and drug discovery (Wang, Baba-Yara, and Chen 2024; Focardi, Fabozzi, and Mazza 2020; Parsons 2011; Cao, Romero, and Aspuru-Guzik 2018). However, in the specific context of few-shot learning, where only limited data is available for training, QML has yet to reach its full potential, often demonstrating suboptimal performance. In classical machine learning, diffusion models have proven effective as zero-shot classifiers and exhibit significant promise in tackling few-shot learning challenges (Li et al. 2023; Clark and Jaini 2024). Nevertheless, the use of quantum diffusion models (QDMs) within QML for few-shot learning remains largely unexplored.(Kölle et al. 2024). This gap is largely attributed to the limitations of current quantum computing resources and the intrinsic noise that hinders the performance of QDMs, despite their demonstrated success in generative tasks(Preskill 2018).

In this work, we propose a suite of novel algorithms based on the QDM framework to address the few-shot learning problem in QML. Our contributions are as follows:

- **Introduction of QDM Based Few-shot Learning Algorithms:** Leveraging the QDM's generative strengths, we present the **QDM based Label-Guided Generation Inference (Qdiff-LGGI)** algorithm, designed specifically for few-shot learning by harnessing label-guided generative capabilities. To further enhance inference during different stages, we introduce two complementary algorithms—**QDM based Label-Guided Noise Addition Inference (Qdiff-LGNAI)** and **QDM based Label-Guided Denoising Inference (Qdiff-LGDI)**—tailored to perform test inference during the diffusion and denoising stages, respectively.
- **Extensive Comparative Analysis:** We evaluate our proposed algorithms across multiple benchmark datasets and compare them against established baselines, demonstrating the superior performance and robustness of our approaches. Additionally, our findings include testing on a real quantum computer, where we analyze the effect of quantum noise on the model's effectiveness.
- **Comprehensive Ablation Study:** We conduct a thorough ablation study to assess the influence of various components and hyperparameters on algorithmic performance. This analysis also extends to examining the potential of our proposed approaches in zero-shot learning, providing insights into their adaptability beyond few-shot contexts.

Background

Quantum Neural Network (QNN). Quantum Neural Networks (QNNs) represent a class of models that extend traditional neural network concepts into the quantum domain, offering powerful computational tools for diverse machine learning tasks. A typical QNN consists of three core components: a data encoder $E(x)$ that maps classical input data x into a quantum state $|x\rangle$, a variational quantum circuit (VQC) Q that manipulates this quantum state to generate a processed output, and a measurement layer M that projects the quantum output back to a classical vector. Various VQC ansatzes commonly used in QNNs are depicted in Fig. 1 (Chu et al. 2022; Sim, Johnson, and Aspuru-Guzik 2019; Patel, Silver, and Tiwari 2022; Wang et al. 2022).

During training, classical data x is transformed into a quantum input feature map via $E(x)$, enabling quantum operations to act directly on encoded features. A parameterized VQC then applies unitary transformations to manipulate this quantum feature representation. The final output is obtained by measuring the output quantum state. The model is trained by minimizing a predefined loss function that quantifies the difference between the QNN's output and the target label y. This training process involves hybrid quantum-classical

[*]This work was conducted when R.W. was an intern at MERL.

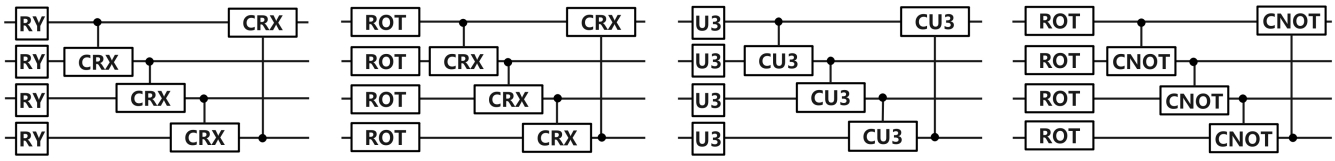

(a)C14 (b)QMLP (c) Quantumnat (d)OPTIC

Figure 1: Various types of variational quantum circuits (VQC) commonly used in Quantum Neural Networks.

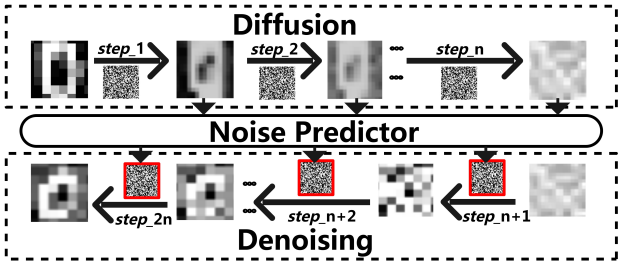

Figure 2: Framework of the Quantum Denoising Diffusion Model (QDDM). The **Noise Predictor** estimates noise present in the noisy image data.

optimization, where parameters in the VQC are iteratively updated to minimize the loss.

Few-Shot Learning (FSL). FSL addresses the challenge of performing supervised learning with limited labeled data(Sun et al. 2019; Parnami and Lee 2022). It is typically structured around two main sets: a support set, containing a small number of labeled examples across n classes with k examples per class (known as n-way k-shot learning), and a query set, which contains unlabeled examples that the model must classify into one of the n classes. Solutions to FSL generally fall into data-based, model-based, and algorithm-based approaches (Wang et al. 2020).

Quantum Few-Shot Learning (QFSL). QFSL leverages QNNs as classifiers to tackle few-shot learning tasks within the quantum realm (Liu et al. 2022; Wang, Richerme, and Chen 2023). However, conventional QFSL algorithms often struggle with performance limitations due to the constraints of quantum computing resources and the presence of noise in quantum hardware, which can reduce model effectiveness. Overcoming these challenges is key to advancing the applicability of QFSL in practical quantum machine learning scenarios.

Diffusion Model (DM). Diffusion models (Ho, Jain, and Abbeel 2020; Song, Meng, and Ermon 2020) are generative models designed to produce high-dimensional data, such as images. A diffusion model operates through two primary processes: the diffusion process, which gradually adds noise to the data over multiple steps, transforming it into a simpler distribution, and the denoising process, which reverses this noise to reconstruct the original data. The diffusion process is defined by

$$q(x_t|x_{t-1}) = \mathcal{N}(x_t; \sqrt{1-\beta_t}x_{t-1}, \beta_t\mathbf{I}) \quad (1)$$

where $\mathcal{N}(\cdot; \mu, \Sigma)$ is a normal distribution with mean μ and covariance Σ, β_t controls the noise level added at step t, and $\mathbf{I}$ is the identity matrix.

In the denoising process, the model learns to reverse this noise addition, progressively reconstructing the data from the noisy state back to its original form. The training objective for the denoising process is given by

$$\mathbb{E}_{q(x_{0:T})}\left[\sum_{t=1}^{T} D_{\mathrm{KL}}\big(q(x_{t-1}|x_t, x_0)\|p_\theta(x_{t-1}|x_t)\big)\right], \quad (2)$$

where $q(x_{t-1}|x_t, x_0)$ is the posterior distribution in the forward diffusion process, and the model $p_\theta(x_{t-1}|x_t)$ predicts the data point from the previous step given the current noisy data. The denoising distribution is defined by

$$p_\theta(x_{t-1}|x_t) = \mathcal{N}\big(x_{t-1}; \mu_\theta(x_t, t), \Sigma_\theta(x_t, t)\big). \quad (3)$$

Quantum Diffusion Model (QDM). The QDM extends diffusion models to the quantum domain, integrating quantum machine learning (QML) with diffusion models for generative tasks, such as quantum state generation and quantum circuit design. The Quantum Denoising Diffusion Model (QDDM) (Kölle et al. 2024) is a leading approach in this field, surpassing classical models of similar size by harnessing the computational advantages of quantum mechanics. Fig. 2 presents the QDDM framework, while Fig. 4 illustrates its image generation process under label guidance.

Our work augments the Quantum Diffusion Model (QDM) with a label-guided mechanism, enhancing its capability to tackle Quantum Few-Shot Learning (QFSL) tasks. This extension incorporates an additional qubit and applies a Pauli-X rotation by an angle of $\frac{2\pi y}{n}$, where y denotes the target label and n represents the total number of classes. Leveraging QDDM's state-of-the-art performance, we adopt it as the foundational QDM framework in this study. Our implementation includes multiple strongly entangling layers, illustrated in Figure 3. The Quantum Neural Network (QNN) architecture within QDDM is further tailored to each dataset by adjusting the number of entangled layers, aligning with the dataset's complexity. Additional configuration details are provided in Section .

Method

To address QFSL challenges, we propose methods from both data and algorithmic perspectives. From the data perspective, we leverage QDDM to augment the training samples, using the generated data to enhance QNN training and thereby improve its prediction accuracy on real data. From an algorithmic standpoint, we employ two strategies to guide QDDM in completing the inference process across two distinct stages: diffusion and denoising.

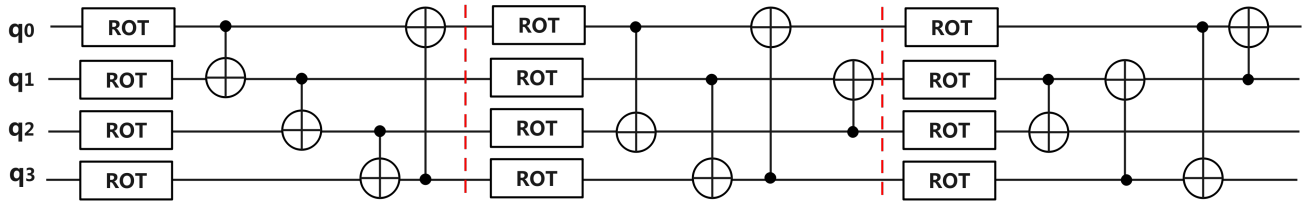

Figure 3: Illustration of a four-qubit strongly entangled layer, with red lines marking the layer boundaries.

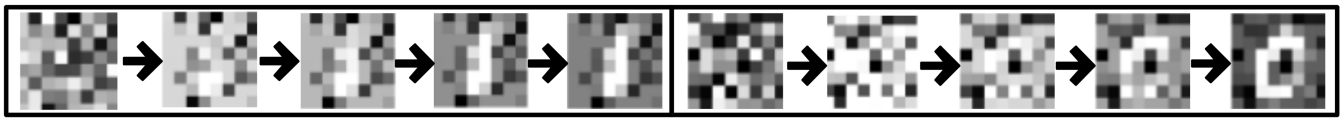

Figure 4: Generated images using QDDM under the guidance of different labels. The input to the model is random noise, which is progressively transformed into label-specific images.

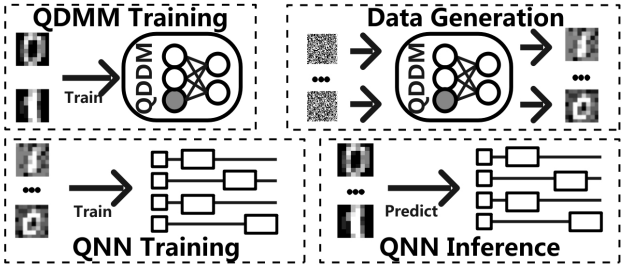

Figure 5: Framework of QDDM-based Label-Guided Generation Inference (QDiff-LGGI). The gray-filled circle represents the embedded label.

QDiff-Based Label-Guided Generation Inference (QDiff-LGGI)

In Quantum Few-Shot Learning (QFSL), the limited availability of labeled training data often hampers the performance of Quantum Neural Networks (QNNs). To address this limitation, expanding the training dataset through data augmentation techniques is essential for enhancing model accuracy and robustness. Leveraging the Quantum Denoising Diffusion Model (QDDM), known for its strong generative capabilities, provides a powerful solution to augment the dataset effectively in QFSL tasks.

The QDiff-LGGI algorithm is designed to maximize QFSL outcomes by generating high-quality, label-guided synthetic data. Initially, we leverage a separate pretrained dataset to conduct the QDDM's pretraining, followed by fine-tuning on a small subset of labeled data. Once fine-tuned, the QDDM acts as a generative model, producing additional samples that closely approximate the distribution of the original data. These synthetic samples are incorporated into the training set, expanding the dataset used to train the QNN. This augmentation process leads to a more comprehensive dataset, which enhances the QNN's inference accuracy on real-world data by improving its generalization to unseen examples.

To further refine the data generated by the QDDM, we employ a label-guided generation technique. During QDDM training, amplitude encoding is applied to represent classical data in the quantum state space, while angle encoding is used to embed label information. In the generation phase, random noise combined with a specified label is provided as input to the QDDM, which generates data aligned with that label. This method ensures that the synthetic data is label-specific, which increases the QNN's ability to distinguish between classes accurately.

Fig. 4 illustrates the data generation process for different label-guidance scenarios, showing how label-specific data distributions are created. Fig. 5 presents the framework of the QDiff-LGGI algorithm in detail, highlighting the integration of label guidance into the QDDM's generative process to produce targeted data for QFSL.

QDiff-Based Label-Guided Noise Addition Inference (QDiff-LGNAI)

The learning objective of the Quantum Denoising Diffusion Model (QDDM), as defined in Equation 2, relies on the accuracy of a noise predictor to estimate and reduce noise within noisy data, aiming to minimize the discrepancy between predicted noise and actual noise. In QDiff-LGNAI, this noise prediction process is guided by label information, where each label is associated with a unique noise prediction that reflects the characteristics of that label. By applying the correct label guidance, the error between the predicted and actual noise can be minimized, thus improving inference accuracy. Based on this principle, we introduce the QDiff-Based Label-Guided Noise Addition Inference (QDiff-LGNAI) method, illustrated in Fig. 6.

The QDiff-LGNAI process begins with finetuning the QDDM on a small subset of labeled data. Once trained, the noise predictor $\mathcal{P}$ within the QDDM is used for inference. Given an input x_0, with potential labels $\{L_1, L_2, \ldots, L_m\}$, noise is progressively added to x_0 across $\mathcal{T}$ iterations to simulate various levels of data degradation. At each time step t, the noisy data x_t is calculated as $x_{t-1} + \epsilon_t$, where $\epsilon_t \sim \mathcal{N}(x_{t-1}, \mathcal{W}[t])$, and $\mathcal{W}$ is a weight matrix that controls the magnitude of noise added at each step.

The noise predictor $\mathcal{P}$ is then used to estimate the noise in x_t for each label, producing a set of label-specific noise predictions $\{\mathcal{P}(x_t|L_1), \ldots, \mathcal{P}(x_t|L_m)\}$. This label-guided

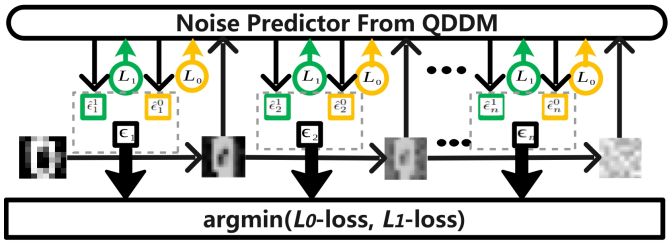

Figure 6: Framework of QDDM-based Label-Guided Noise Addition Inference (QDiff-LGNAI). The term $\hat{\epsilon}_m^n$ represents the predicted noise at step m associated with label n. L_0/L_1-loss denotes the difference between true noise and the predicted noise under the guidance of different labels L_i.

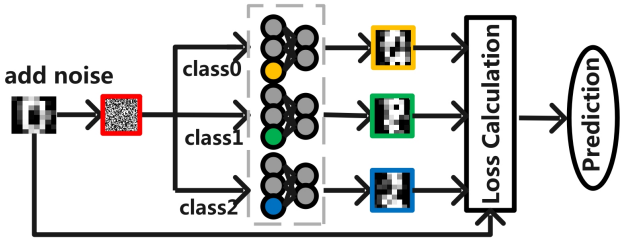

Figure 7: Framework of QDDM-based Label-Guided Denoising Inference (QDiff-LGDI). Solid circles in different colors represent distinct embedded labels. The output images, each framed by a square of varying colors, indicate the generated images guided by different labels L_i.

noise prediction allows QDiff-LGNAI to evaluate how well each label aligns with the observed noisy data.

To identify the correct label, we calculate the mean squared error (MSE) between each predicted noise value $\mathcal{P}(x_t|L_i)$ and the actual noise ϵ_t. By minimizing this discrepancy, QDiff-LGNAI aims to select the label that most accurately explains the noisy data across all $\mathcal{T}$ iterations. The label with the minimum cumulative error over $\mathcal{T}$ time steps is chosen as the predicted label, as shown below:

$$\arg\min_{L_i \in \mathcal{L}} \sum_{t=1}^{\mathcal{T}} \text{MSE}(\mathcal{P}(x_t|L_i), \epsilon_t).$$

This approach leverages the QDDM's ability to capture label-specific noise patterns, allowing QDiff-LGNAI to enhance classification accuracy even in the presence of noisy inputs. By aligning predicted noise with actual noise under different label conditions, QDiff-LGNAI improves the robustness of QFSL applications, especially where noisy data is prevalent.

QDiff-Based Label-Guided Denoising Inference (QDiff-LGDI)

The QDiff-Based Label-Guided Denoising Inference (QDiff-LGDI) method leverages the denoising capabilities of the Quantum Denoising Diffusion Model (QDDM) to iteratively restore noisy data, steering it toward its original structure. In QDiff-LGDI, the QDDM's noise predictor estimates the noise in each sample and iteratively subtracts it over a series of steps. By introducing label-specific guidance at each denoising step, QDiff-LGDI ensures that the data generated under the correct label aligns most closely with the original data, enhancing the accuracy of inference.

Starting with an initial input x_0, noise is incrementally added across $\mathcal{T}$ iterations, producing a sequence of progressively noisier data points $\{x_1, x_2, \ldots, x_\mathcal{T}\}$. For each noisy data point, the QDDM's noise predictor $\mathcal{P}$ estimates the noise under a specified label L_i, with $\mathcal{P}(x_\mathcal{T}|L_i)$ representing the label-guided noise estimate. This predicted noise is then subtracted iteratively, resulting in progressively denoised data points $\{x_{\mathcal{T}+1}, x_{\mathcal{T}+2}, \ldots, x_{2\mathcal{T}}\}$, where each denoising step is defined by:

$$x_{\mathcal{T}+t+1}|L_i = x_{\mathcal{T}+t} - \mathcal{P}(x_{\mathcal{T}+t}|L_i).$$

This iterative denoising sequence ultimately reconstructs a fully restored version of the data, with the goal of identifying the label L_i that provides the most accurate denoising guidance. This label selection ensures that the denoised output aligns as closely as possible with the original data state prior to noise addition.

To determine the correct label, QDiff-LGDI calculates the Mean Squared Error (MSE) between each denoised data point $x_{2\mathcal{T}-t}|L_i$ and the corresponding noisy data point x_t, aggregated across all $\mathcal{T}$ iterations. This cumulative MSE provides a measure of discrepancy between the generated data and the original data for each label. The label that minimizes this cumulative error over all denoising steps is chosen as the most accurate:

$$\arg\min_{L_i \in \mathcal{L}} \sum_{t=0}^{\mathcal{T}} \text{MSE}(x_t, x_{2\mathcal{T}-t}|L_i).$$

By aligning noise prediction with label-specific guidance, QDiff-LGDI empowers the QDDM to generate data that is both accurate and closely aligned with the correct label. This approach is particularly advantageous in scenarios requiring fine distinctions between closely related classes, as it leverages subtle label-specific variations in noise characteristics. This label-guided denoising technique refines the QFSL algorithm's classification performance, enhancing its capacity to discern nuanced patterns within noisy data environments.

Experiment

In this section, we outline the foundational settings of our experimental setup, detailing the datasets, baseline algorithms, and parameter configurations. Each of these components is crucial for assessing the performance of our proposed QDiff-based algorithms in quantum few-shot learning (QFSL). We further conduct a series of experiments to address the following research questions, with each question explored in its respective subsection:

- What are the performance advantages of our proposed QDiff-based algorithms compared to existing baseline methods?

Table 1: QNN structures used in the few-shot learning task. The variable n indicates the number of layers in the QNN, with a default of $n = 1$.

QNN	# Qubits	1QG	2QG	# Param.
QMLP	6	ROT	CRX	$24 \times n$
C14	6	RY	CRX	$12 \times n$
OPTIC	6	ROT	CNOT	$18 \times n$
Quantumnat	6	U3	CU3	$36 \times n$

- Which factors most significantly influence the performance of our algorithms?
- How effectively do our algorithms address the zero-shot learning problem?

Basic Experimental Settings

We begin by providing a detailed description of the datasets utilized, the baseline algorithms chosen, and the specific configurations applied in our experiments.

Dataset. For our experiments, we utilize the Digits MNIST (Alpaydin and Alimoglu 1996), MNIST (LeCun et al. 1998), and Fashion MNIST (Xiao 2017) datasets, which allow for a comprehensive assessment of our algorithms across varied data characteristics. For the 2-way k-shot tasks, we select classes 0 and 1 from both Digits MNIST and MNIST, and the T-shirt and Trouser classes from Fashion MNIST. In the 3-way k-shot tasks, we include classes 0, 1, and 2 from Digits MNIST and MNIST, and the T-shirt, Trouser, and Pullover classes from Fashion MNIST. The remaining categories in each dataset are reserved for QDDM pretraining; for example, classes 4–9 in MNIST are used to pretrain QDDM for evaluating QDiff-based QFSL algorithms on MNIST. To simulate few-shot learning, we use one image per class for one-shot tasks and ten images per class for ten-shot tasks. During inference, each class is represented by 200 images in the evaluation dataset. For computational efficiency, all images are resized to 8×8.

Baselines and Parameter Settings. To rigorously evaluate the performance of our QDiff-based algorithms against established benchmarks, we select four prominent Quantum Neural Network (QNN) architectures that are widely employed in quantum machine learning (QML) for quantum few-shot learning (QFSL) tasks (Chu et al. 2022; Sim, Johnson, and Aspuru-Guzik 2019; Patel, Silver, and Tiwari 2022; Wang et al. 2022). These architectures are depicted in Figure 1, providing a visual overview, while detailed specifications, including their structural configurations and parameter settings, are summarized in Table 1. During training, classical data is mapped to quantum states using amplitude encoding, ensuring efficient representation within the quantum framework. Optimization is conducted via the Adam optimizer, with a learning rate fixed at 0.001, to minimize the cross-entropy loss function over 40 iterations, providing a robust foundation for comparative analysis.

QDDM Training. Before applying the QDiff-based algorithms to the QFSL tasks, we pre-train the Quantum Denoising Diffusion Model (QDDM) using a label-guided, quantum-dense architecture. Labels are encoded through RX rotations, and strongly entangling layers (Bergholm et al. 2018) are utilized to effectively process the data. The training process employs the Adam optimizer over $10{,}000$ iterations. To further enhance the QDDM's performance, the architecture is fine-tuned to extract critical features from the input images.

The depth of the Quantum Neural Network (QNN) within QDDM significantly influences its feature extraction capabilities. While deeper architectures often provide superior feature representations, excessive depth may lead to barren plateaus that impede effective training. To address this challenge, we carefully design the model architecture and optimize the learning rate for each dataset. Table 2 summarizes the specific training configurations applied across datasets, forming the basis of our evaluation of the QDiff-based algorithms in few-shot learning tasks.

By meticulously configuring and pre-training the QDDM model and selecting robust QNN baselines, we aim to provide a comprehensive assessment of the efficacy and reliability of the proposed methods. Figure 8 illustrates the training loss trend as QDDM is trained on the Digits MNIST dataset. The progressive decrease in training loss over time reflects the enhanced accuracy of the noise predictor in estimating noise levels, resulting in increasingly denoised images that closely align with the target images.

During the fine-tuning phase, we utilize a small dataset to refine the model over 100 iterations, maintaining the same learning rate as used in the initial training phase.

Table 2: Parameter configurations used in QDDM training. **LR** denotes the learning rate, while **Diff-Step** specifies the number of diffusion steps.

Dataset	Model Shape	LR	Diff-Step
Digit MNIST	47 layers	0.00097	10
MNIST	60 layers	0.00211	10
Fashion MNIST	121 layers	0.00014	10

Performance Analysis of QDiff-based QFSL Algorithms

In the structured n-way, k-shot configuration, we systematically sample k images from each of n distinct categories, amassing a comprehensive dataset of $n \times k$ training images. These images are subsequently utilized to complete the fine-tuning of the QDDM. The fine-tuned model is then integrated into the QDiff-based algorithms, enhancing their performance and adaptability in diverse quantum few-shot learning scenarios.

Table 3 presents a detailed performance comparison of the QDiff-based Quantum Few-Shot Learning (QFSL) algorithms against established baseline methods within varied scenarios: 2-way 1-shot, 2-way 10-shot, 3-way 1-shot, and 3-way 10-shot. The outcomes clearly indicate that the QDiff-based algorithms consistently deliver state-of-the-art performance, thereby confirming their superior efficacy in few-shot learning applications. Furthermore, we evaluate the resilience of the QDiff-based algorithms in a practical setting by testing them on a 3-way, 1-shot task using the Digits MNIST dataset on the IBM_Almaden quantum processor. As

Table 3: Performance comparison of QDiff-based algorithms across various tasks, with $\mathcal{T} = 5$. Each algorithm is evaluated using 5 random seeds to report mean performance and standard error. The best-performing algorithm for each task is highlighted in blue.

Dataset	Tasks	QDiff-LGDI	QDiff-LGNAI	QDiff-LGGI	QMLP	C14	OPTIC	Quantumnat
Digits	2w-01s	$0.975_{\pm 0.059}$	$0.978_{\pm 0.003}$	$0.992_{\pm 0.009}$	$0.764_{\pm 0.108}$	$0.505_{\pm 0.175}$	$0.525_{\pm 0.133}$	$0.751_{\pm 0.147}$
	2w-10s	$0.983_{\pm 0.006}$	$0.997_{\pm 0.002}$	$0.984_{\pm 0.012}$	$0.892_{\pm 0.086}$	$0.627_{\pm 0.086}$	$0.886_{\pm 0.193}$	$0.722_{\pm 0.186}$
	3w-01s	$0.525_{\pm 0.001}$	$0.635_{\pm 0.007}$	$0.573_{\pm 0.069}$	$0.338_{\pm 0.087}$	$0.447_{\pm 0.193}$	$0.475_{\pm 0.021}$	$0.555_{\pm 0.013}$
	3w-10s	$0.857_{\pm 0.015}$	$0.801_{\pm 0.008}$	$0.632_{\pm 0.035}$	$0.355_{\pm 0.059}$	$0.481_{\pm 0.183}$	$0.698_{\pm 0.121}$	$0.687_{\pm 0.156}$
MNIST	2w-01s	$0.943_{\pm 0.002}$	$0.965_{\pm 0.003}$	$0.805_{\pm 0.093}$	$0.675_{\pm 0.067}$	$0.567_{\pm 0.064}$	$0.845_{\pm 0.149}$	$0.701_{\pm 0.162}$
	2w-10s	$0.953_{\pm 0.011}$	$0.978_{\pm 0.005}$	$0.915_{\pm 0.079}$	$0.817_{\pm 0.048}$	$0.810_{\pm 0.152}$	$0.807_{\pm 0.173}$	$0.727_{\pm 0.151}$
	3w-01s	$0.475_{\pm 0.003}$	$0.505_{\pm 0.007}$	$0.428_{\pm 0.035}$	$0.325_{\pm 0.027}$	$0.503_{\pm 0.122}$	$0.477_{\pm 0.159}$	$0.501_{\pm 0.012}$
	3w-10s	$0.720_{\pm 0.016}$	$0.825_{\pm 0.008}$	$0.405_{\pm 0.022}$	$0.547_{\pm 0.085}$	$0.607_{\pm 0.142}$	$0.770_{\pm 0.191}$	$0.527_{\pm 0.078}$
Fashion	2w-01s	$0.738_{\pm 0.007}$	$0.768_{\pm 0.007}$	$0.898_{\pm 0.036}$	$0.688_{\pm 0.064}$	$0.581_{\pm 0.187}$	$0.765_{\pm 0.149}$	$0.583_{\pm 0.181}$
	2w-10s	$0.755_{\pm 0.020}$	$0.805_{\pm 0.002}$	$0.895_{\pm 0.066}$	$0.731_{\pm 0.035}$	$0.773_{\pm 0.099}$	$0.793_{\pm 0.157}$	$0.887_{\pm 0.129}$
	3w-01s	$0.453_{\pm 0.008}$	$0.433_{\pm 0.001}$	$0.483_{\pm 0.012}$	$0.331_{\pm 0.098}$	$0.332_{\pm 0.172}$	$0.473_{\pm 0.128}$	$0.622_{\pm 0.063}$
	3w-10s	$0.655_{\pm 0.018}$	$0.735_{\pm 0.004}$	$0.585_{\pm 0.025}$	$0.647_{\pm 0.015}$	$0.527_{\pm 0.173}$	$0.593_{\pm 0.139}$	$0.653_{\pm 0.032}$
Average		$0.754_{\pm 0.015}$	$0.795_{\pm 0.004}$	$0.719_{\pm 0.045}$	$0.574_{\pm 0.060}$	$0.546_{\pm 0.140}$	$0.678_{\pm 0.150}$	$0.666_{\pm 0.120}$

illustrated in Fig. 10, despite the inherent noise challenges of quantum hardware, the performance degradation observed is marginal. This finding underscores the robustness of our algorithms, maintaining high accuracy in adverse quantum environments and demonstrating their strong potential for real-world deployment on quantum computing platforms.

Factors Impacting the Effectiveness of QDiff-based QFSL Algorithms

This section investigates key factors that affect the performance of QDiff-based algorithms, including the influence of diffusion and denoising step counts, the quantity and diversity of training data, and the selection of QNNs used in QDiff-LGGI.

Impact of Diffusion and Denoising Steps. The calibration of diffusion and denoising steps is crucial in shaping the quality of the generated images, which in turn significantly impacts the inference accuracy of QDiff-based algorithms. As depicted in Fig. 9, modifying the step count leads to significant performance variations on the Digits MNIST and MNIST datasets. Our experiments highlight that QDiff-LGGI is notably responsive to changes in these steps. Increasing the number of steps generally improves the fidelity of the images to the target data distribution, thereby enhancing inference performance. However, an excessive number of steps can result in substantial degradation of the initial image into noise during the diffusion process, complicating the subsequent reconstruction in the denoising phase. This can result in the reconstruction algorithm overly emphasizing the guiding label, creating discrepancies with the original image—a challenge particularly pronounced in QDiff-LGNAI and QDiff-LGDI. This observation underscores the critical need for a judicious balance in step count to optimize inference accuracy effectively.

Effect of Training Data Quantity. The volume of training data critically affects the performance of QDiff-based QFSL algorithms, directly influencing the quality and efficacy of the QDDM model. This study compares one-shot and ten-shot learning scenarios across various datasets, with detailed performance metrics consolidated in Table 3. The findings affirm that an increased volume of training data substantially benefits the training of the QDDM model, fostering more nuanced representations and enabling the generation of more precise and varied samples. Consequently, QDiff-based algorithms exhibit enhanced inference accuracy with a well-trained QDDM model, accentuating the significance of ample and representative training data in few-shot learning tasks.

Choice of QNN Architecture. The architecture of the QNN employed within QDiff-LGGI profoundly influences inference performance by determining the model's representational and generalization capabilities. QDiff-LGGI utilizes images generated by QDDM to train the QNN, which is then employed for inference tasks. As illustrated in Fig. 11, the inference accuracy notably varies across different QNN architectures, potentially attributable to variations in circuit expressibility and entangling capabilities, as noted in (Sim, Johnson, and Aspuru-Guzik 2019). Certain QNN architectures may offer more robust representations of the input data, capturing complex relationships with greater fidelity and thus yielding superior performance in QFSL tasks. This insight highlights the importance of selecting an appropriate QNN architecture that aligns with the complexity of the task and the characteristics of the data to maximize the effectiveness of QDiff-LGGI.

Zero-Shot Learning with QDiff-based QFSL Algorithms

We explore the efficacy of our QDiff-based algorithms in addressing zero-shot learning tasks, where no prior examples from the evaluation classes are available during training. To assess this capability, we perform evaluations between two datasets with closely aligned data distributions: Digit MNIST and MNIST. Given the challenges posed by quantum diffusion models and limited hardware resources, these datasets provide an ideal testbed to verify cross-domain generalization in zero-shot settings. We conduct the following verifications:

- **Verification of QDiff-LGDI Performance in Zero-Shot Learning:** This setup aims to assess the generalization capacity of QDiff-LGDI when a QNN is trained on data

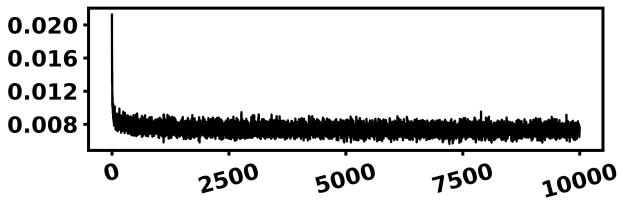

Figure 8: Training Loss Trends during QDDM Model Training.

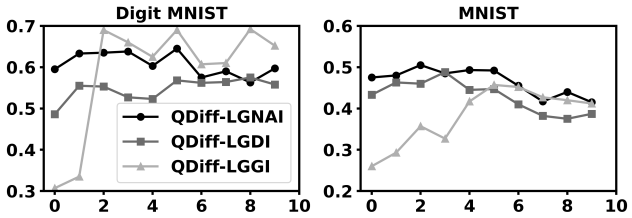

Figure 9: Performance of QDiff-based algorithms on the 3-way, 1-shot task under varying diffusion and denoising step configurations.

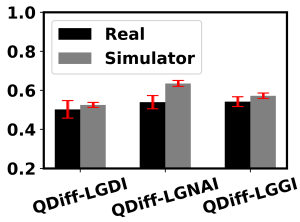

Figure 10: Performance of QDiff-based algorithms for the 3-way, 1-shot task on IBM_Almaden.

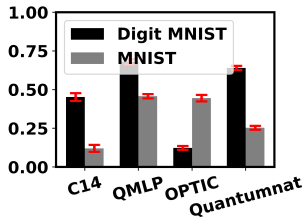

Figure 11: Performance of QDiff-LGGI on the 3-way, 1-shot task across different QNNs.

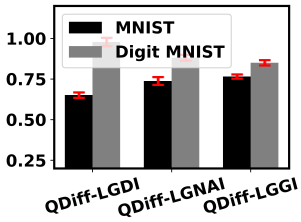

Figure 12: Performance of QDiff-based algorithms on the zero-shot, two-class classification task.

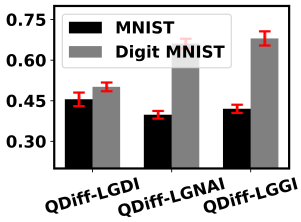

Figure 13: Performance of QDiff-based algorithms on the zero-shot, three-class classification task.

generated by QDDM from one domain and subsequently applied to another.

- **Digit MNIST:** The QDDM model is trained on the MNIST dataset, where an augmented dataset is generated for QNN training. After training the QNN, it is used to perform inference on the Digit MNIST dataset to evaluate cross-domain generalization.
- **MNIST:** The QDDM model is trained on the Digit MNIST dataset, with the augmented dataset used for QNN training. The trained QNN is then applied to the MNIST dataset for inference, allowing us to evaluate generalization in the reverse direction.

- **Verification of QDiff-LGNAI and QDiff-LGGI Performance in Zero-Shot Learning:** This evaluation tests the direct applicability of QDiff-LGNAI and QDiff-LGGI algorithms in zero-shot settings without retraining the QNN on new data.
  - **Digit MNIST:** The QDDM model is trained on the MNIST dataset and directly applied for inference on the Digit MNIST dataset, examining the robustness of the QDiff-LGNAI and QDiff-LGGI algorithms in adapting to unseen yet similar data distributions.
  - **MNIST:** Similarly, the QDDM model is trained on the Digit MNIST dataset and subsequently applied directly for inference on the MNIST dataset, assessing the generalization potential of these algorithms in the reverse direction.

Figs. 12 and 13 illustrate the performance results for the zero-shot tasks across these configurations. The results demonstrate that QDiff-based algorithms achieve strong zero-shot learning performance, particularly when the source and target datasets exhibit similar data structures and distributions. These findings underscore the robustness and adaptability of QDiff-based QFSL algorithms, showcasing their potential to generalize effectively across related domains even in the absence of target domain data during training.

Conclusion and Future Work

In this work, we present the quantum diffusion model (QDM) as a pioneering approach to overcome the unique challenges of quantum few-shot learning (QFSL). We introduce three novel algorithms—QDiff-LGDI, QDiff-LGNAI, and QDiff-LGGI—developed from complementary data-driven and algorithmic perspectives to enhance the performance of QFSL tasks. Through extensive experimentation, we demonstrate that these algorithms achieve significant performance gains over traditional baselines, underscoring the potential of QDM to advance QFSL by effectively leveraging quantum noise modeling and label guidance.

While the results are promising, our current implementation of QDM faces limitations, particularly in its scalability to more complex datasets and real-world quantum applications. These constraints highlight the need for further research to unlock the full potential of QDM. Future work could focus on extending the capabilities of QDM through improvements in model architecture and optimization techniques, enabling it to handle more intricate datasets with diverse and high-dimensional features.

Moreover, expanding QDM's applicability across additional quantum machine learning (QML) domains presents exciting opportunities. Potential directions include quantum object detection, quantum semantic segmentation, and other advanced generative tasks where QDM's noise-guided diffusion and label-conditional modeling could provide significant advantages. Integrating QDM into these areas would not only broaden its utility but could also position it as a versatile and foundational framework for future quantum learning architectures. By advancing QDM's robustness and adaptability, this line of research has the potential to transform QML applications and contribute meaningfully to the field of quantum artificial intelligence.

References

Alpaydin, E.; and Alimoglu, F. 1996. Pen-Based Recognition of Handwritten Digits. UCI Machine Learning Repository. DOI: https://doi.org/10.24432/C5MG6K.

Bergholm, V.; Izaac, J.; Schuld, M.; Gogolin, C.; Ahmed, S.; Ajith, V.; Alam, M.; Alonso-Linaje, G.; AkashNarayanan, B.; Asadi, A.; et al. 2018. Pennylane: Automatic differentiation of hybrid quantum-classical computations. arXiv 2018. *arXiv preprint arXiv:1811.04968*.

Cao, Y.; Romero, J.; and Aspuru-Guzik, A. 2018. Potential of quantum computing for drug discovery. *IBM Journal of Research and Development*, 62(6): 6–1.

Chu, C.; Chia, N.-H.; Jiang, L.; and Chen, F. 2022. Qmlp: An error-tolerant nonlinear quantum mlp architecture using parameterized two-qubit gates. In *Proceedings of the ACM/IEEE International Symposium on Low Power Electronics and Design*, 1–6.

Clark, K.; and Jaini, P. 2024. Text-to-image diffusion models are zero shot classifiers. *Advances in Neural Information Processing Systems*, 36.

Focardi, S.; Fabozzi, F. J.; and Mazza, D. 2020. Quantum option pricing and quantum finance. *Journal of Derivatives*, 28(1): 79–98.

Ho, J.; Jain, A.; and Abbeel, P. 2020. Denoising diffusion probabilistic models. *Advances in neural information processing systems*, 33: 6840–6851.

Kölle, M.; Stenzel, G.; Stein, J.; Zielinski, S.; Ommer, B.; and Linnhoff-Popien, C. 2024. Quantum Denoising Diffusion Models. *arXiv preprint arXiv:2401.07049*.

LeCun, Y.; Bottou, L.; Bengio, Y.; and Haffner, P. 1998. Gradient-based learning applied to document recognition. *Proceedings of the IEEE*, 86(11): 2278–2324.

Li, A. C.; Prabhudesai, M.; Duggal, S.; Brown, E.; and Pathak, D. 2023. Your diffusion model is secretly a zero-shot classifier. In *Proceedings of the IEEE/CVF International Conference on Computer Vision*, 2206–2217.

Liu, M.; Liu, J.; Liu, R.; Makhanov, H.; Lykov, D.; Apte, A.; and Alexeev, Y. 2022. Embedding learning in hybrid quantum-classical neural networks. In *2022 IEEE International Conference on Quantum Computing and Engineering (QCE)*, 79–86. IEEE.

Parnami, A.; and Lee, M. 2022. Learning from few examples: A summary of approaches to few-shot learning. *arXiv preprint arXiv:2203.04291*.

Parsons, D. F. 2011. Possible medical and biomedical uses of quantum computing. *Neuroquantology*, 9(3).

Patel, T.; Silver, D.; and Tiwari, D. 2022. OPTIC: A practical quantum binary classifier for near-term quantum computers. In *2022 Design, Automation & Test in Europe Conference & Exhibition (DATE)*, 334–339. IEEE.

Preskill, J. 2018. Quantum computing in the NISQ era and beyond. *Quantum*, 2: 79.

Sim, S.; Johnson, P. D.; and Aspuru-Guzik, A. 2019. Expressibility and entangling capability of parameterized quantum circuits for hybrid quantum-classical algorithms. *Advanced Quantum Technologies*, 2(12): 1900070.

Song, J.; Meng, C.; and Ermon, S. 2020. Denoising diffusion implicit models. *arXiv preprint arXiv:2010.02502*.

Sun, Q.; Liu, Y.; Chua, T.-S.; and Schiele, B. 2019. Meta-transfer learning for few-shot learning. In *Proceedings of the IEEE/CVF conference on computer vision and pattern recognition*, 403–412.

Wang, H.; Gu, J.; Ding, Y.; Li, Z.; Chong, F. T.; Pan, D. Z.; and Han, S. 2022. Quantumnat: quantum noise-aware training with noise injection, quantization and normalization. In *Proceedings of the 59th ACM/IEEE design automation conference*, 1–6.

Wang, R.; Baba-Yara, F.; and Chen, F. 2024. JustQ: Automated deployment of fair and accurate quantum neural networks. In *2024 29th Asia and South Pacific Design Automation Conference (ASP-DAC)*, 121–126. IEEE.

Wang, R.; Richerme, P.; and Chen, F. 2023. A hybrid quantum–classical neural network for learning transferable visual representation. *Quantum Science and Technology*, 8(4): 045021.

Wang, Y.; Yao, Q.; Kwok, J. T.; and Ni, L. M. 2020. Generalizing from a few examples: A survey on few-shot learning. *ACM computing surveys (csur)*, 53(3): 1–34.

Xiao, H. 2017. Fashion-mnist: a novel image dataset for benchmarking machine learning algorithms. *arXiv preprint arXiv:1708.07747*.